Electronic structure, spin couplings, and hyperfine properties of nanoscale molecular magnets

Z. Zeng
Institute of Solid State Physics, Academia Sinica, Hefei 230031, People's Republic of China

Diana Guenzburger
Centro Brasileiro de Pesquisas Físicas, rua Xavier Sigaud 150, 22290-180 Rio de Janeiro, Rio de Janeiro, Brazil

D. E. Ellis
Department of Physics and Astronomy and Materials Research Center, Northwestern University, Evanston, Illinois 60208
(Received 8 September 1998)

First-principles self-consistent spin-polarized electronic structure calculations were performed for the nanoscale magnetic molecules $Mn_{12}O_{12}(CH_3COO)_{16}(H_2O)_4$ and $Fe_{11}O_6(OH)_6(O_2CPh)_{15}$. The numerical discrete variational method was employed, within density-functional theory. Charges and magnetic moments were obtained for the atoms, as well as density of states diagrams, and charge- and spin-density maps. For $Mn_{12}O_{12}(CH_3COO)_{16}(H_2O)_4$, values of the Heisenberg exchange parameters J were derived from the calculations; Mössbauer hyperfine parameters were calculated for $Fe_{11}O_6(OH)_6(O_2CPh)_{15}$ and compared to reported experimental values. [S0163-1829(99)05709-4]

I. INTRODUCTION

Clusters of nanoscale or mesoscopic dimensions containing transition elements and oxygen have attracted a great deal of attention recently, for a variety of reasons. From the biological point of view, clusters comprising transition-metal ions exist in several metalloenzymes and metalloproteins,[1] as in the water oxidizing complex (WOC), involved in bacterial photosynthesis,[2] or ferritin, a protein which stores Fe in mammals and consists of a Fe-O core encapsulated in a polypeptide envelope.[3] Large transition-metal molecular aggregates with well-defined structures may be fabricated experimentally, and serve as models for such biological systems.[4] On the other hand, magnetic transition-metal oxo clusters present new and exciting properties due to their nanoscale dimensions. These systems are on the borderline of the paramagnetic behavior of isolated molecules and collective magnetism of bulk solids, and thus may be considered as forming a different magnetic phase.[5]

We have investigated two important examples of such nanoscale molecules, the mixed-valence Mn complex $Mn_{12}O_{12}(CH_3COO)_{16}(H_2O)_4$ (which we will refer to hereafter as Mn_{12}) and $Fe_{11}O_6(OH)_6(O_2CPh)_{15}$ (referred to as Fe_{11}), from the point of view of the electronic structure.

Mn_{12} is a mixed-valence system since it contains Mn ions with formal charge $+3$ and $+4$, and as such constitutes a model for the biological complex WOC of photosystem II of bacterial photosynthesis.[6–8] Furthermore, many interesting magnetic properties have been demonstrated for this molecule, which crystalizes in a tetragonal structure as determined by Lis in 1980.[9] ac susceptibility, magnetization, and EPR measurements led to the conclusion that each molecule has a total spin $S=10$;[10,11] this large spin combined with a large easy-axis anisotropy leads to superparamagnetic behavior at low temperature, with very long relaxation time which results in pronounced hysteresis.[12] The spins of the individual magnetic ions are coupled strongly together in each molecular unit, which behaves as one small magnet; on the other hand, the magnetic interactions between units are practically negligible, due mainly to the crown of ligands surrounding and isolating the metal-oxo core. These properties make such system a potential candidate for molecular-size-units data storage devices. Many experimental measurements have been reported for this molecule, such as proton NMR and muon spin rotation,[13] neutron diffraction with[14] or without[15] an applied magnetic field, magnetic circular dichroism[16] and high-frequency EPR.[17] A very exciting discovery has been the observation of steps in the hysteresis loop of the magnetization in a powdered sample[18] or single crystals[19] of Mn_{12} at low temperatures. This was interpreted as a manifestation of quantum tunneling in a macroscopic property.

The nanoscale molecule Fe_{11} also forms crystals of well-defined structure,[20] with the molecules containing a Fe-O core surrounded by the organic ligands. This structure forms a model for ferritin. There are three crystallographically different sites for the Fe ions, all in the formal oxidation state $+3$. These molecular aggregates have similar magnetic properties to Mn_{12} in the sense that the individual Fe spins within each molecule couple together strongly resulting in magnetic order. Moreover, Mössbauer spectroscopy measurementsof the hyperfine parameters are available.[20]

The results of the electronic structure calculations provide insight into these nanoscale molecular magnets, and will add to the experimental data to provide a more complete understanding of their properties. A similar theoretical study has been reported for the mesoscopic cluster $[Fe(OMe)_2(O_2CCH_2Cl)]_{10}$, a molecular antiferromagnet denominated ''ferric wheel'' due to its circular arrangement.[21] We have employed the spin-polarized discrete variational method[22] (DVM) of density-functional theory[23] (DFT) to obtain energy levels, charge, and spin densities for Mn_{12} and Fe_{11}. Charges and magnetic moments on the ions are also reported. Hyperfine parameters are calculated for Fe_{11} and

compared to experimental values. Finally, the Heisenberg spin-coupling parameters J are obtained from the calculations for Mn_{12}, employing the magnetic transition state concept.[24]

In Sec. II we describe briefly the method employed, in Sec. III we report the results for Mn_{12}, in Sec. IV the results for Fe_{11}, and in Sec. V we briefly state our main conclusions.

II. THEORETICAL METHOD

The DV method has been extensively described in the literature,[22,21] so here we give only a summary of its main features. We seek to solve the Kohn-Sham equations of density-functional theory[23] for a cluster of atoms or a molecule, in a three-dimensional grid of points:

$$(-\nabla^2/2+V_c+V_{\mathrm{xc}}^{\sigma})\varphi_{i\sigma}=\varepsilon_{i\sigma}\varphi_{i\sigma}. \tag{1}$$

In Eq. (1), V_c is the Coulomb potential of nuclei and electrons, and V_{xc}^{σ} is the spin-dependent exchange-correlation potential, for which we employed the functional of Vosko, Wilk, and Nusair (VWN).[25] The potential is a functional of the electron density of spin σ, obtained from the molecular one-electron functions (or spin-orbitals) $\varphi_{i\sigma}$ by

$$\rho_{\sigma}(\mathbf{r})=\Sigma_i n_{i\sigma}|\varphi_{i\sigma}(\mathbf{r})|^2. \tag{2}$$

$n_{i\sigma}$ are the occupations (0 or 1) of the spin orbitals, filled according to Fermi-Dirac statistics. The spin orbitals are expanded as linear combinations of numerical atomic orbitals (LCAO) χ_j:

$$\varphi_{\sigma i}(\mathbf{r})=\Sigma_j\chi_j(\mathbf{r})c_{i\sigma}^{j}. \tag{3}$$

Minimizing the error function of the DV method leads to secular equations analogous to those of the standard Rayleigh-Ritz variational method:

$$([H]-[E][S])[C]=0, \tag{4}$$

where $[H]$ is the Kohn-Sham Hamiltonian matrix, $[S]$ is the overlap matrix and $[C]$ is the matrix of the coefficients in expansion (3). Since the Hamiltonian depends on the density given by Eq. (2), iterations are performed to solve the secular equations self-consistently in the three-dimensional grid of points. The numerical grid is pseudorandom (diophantine)[22] in all space except inside spheres containing the nuclei and core electrons of the Mn and Fe atoms, where a precise polynomial integration is performed.[26]

A Mulliken-type population analysis,[27] in which the atomic orbital occupancy is obtained from the coefficients in the LCAO expansion, was performed to obtain the configurations of the atoms in the molecules. After a cycle of iterations is completed, the atomic configurations obtained are used in atomic self-consistent numerical DFT calculations to obtain a basis set more adapted to the molecular environment. This procedure is repeated two or three times to optimize the basis. The orbitals included in the valence space are $3s$, $3p$, $3d$, $4s$, and $4p$ for the transition metals, $2s$ and $2p$ for C and O, and $1s$ for H. The core orbitals are kept ''frozen'' throughout the iterations, and the valence orbitals are explicitly orthogonalized to the core in the first iteration. To render tractable the Coulomb electron-electron interaction integral, a model potential is constructed by least-squares fitting the ''real'' charge and spin densities to a multicenter multipolar expansion.[28] In the present calculations, terms up to $l=1$ were included in the expansion. The self-consistent criterion in the present calculations was <0.01 in the expansion coefficients of the model $\rho(\mathbf{r})$. For magnetic systems such as those considered, spin-polarized calculations are performed to obtain magnetic moments and spin densities $[\rho_{\uparrow}(\mathbf{r})-\rho_{\downarrow}(\mathbf{r})]$. This is achieved by allowing the spin-up orbitals to be different from spin down, which will occur as a consequence of the imbalance in the number of electrons of each spin.

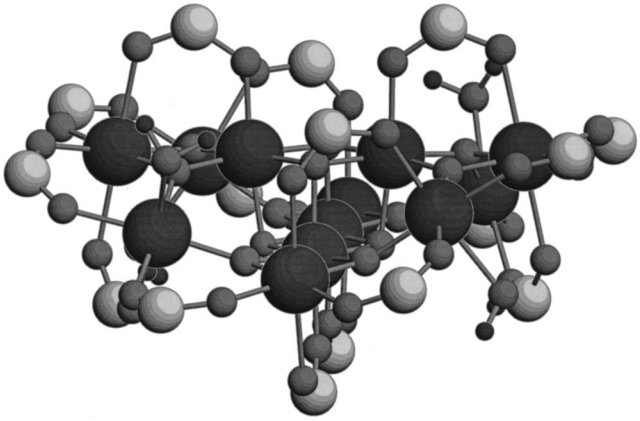

FIG. 1. Representation of $Mn_{12}(CH_3COO)_{16}(H_2O)_4O_{12}$, minus CH_3 ligands. Atoms are represented by spheres according to relative sizes: Mn>C>O>H.

We may comment here on the choice of exchange and correlation potential and the possible utility of hybrid and gradient-corrected functionals. First, the VWN exchange-correlation energy and potential has established itself as a stable and accurate approximation, among the many local spin-density schemes, both in molecules and solids. On the other hand, theoretical developments and empirical fitting procedures give rise to gradient-corrected (GGA) or nonlocal functionals, which have proven to increase the accuracy of predicted bond lengths, binding energies and other properties obtained from total-energy calculations. However, for the properties derived here, such as magnetic moments, spin coupling constants, and hyperfine parameters, no systematic knowledge on the possible improvement brought in by nonlocal functionals is available. For example, it was shown that GGA has little impact on the calculated hyperfine fields of Fe, Co, and Ni metals;[29] in the case of Co and Ni, values found in fact differ more from experiment than those obtained with VWN. More systematic investigations of the effect of nonlocal potentials on such properties are needed.

III. THE MOLECULAR NANOMAGNET $Mn_{12}O_{12}(CH_3COO)_{16}(H_2O)_4$

A. Electronic structure and magnetic properties

As mentioned in the Introduction, the structure of Mn_{12} has been determined by x-ray diffraction;[9] the experimentally determined atomic coordinates reported in the literature were employed in the present calculations.

In Fig. 1 is given a representation of the Mn_{12} molecule,

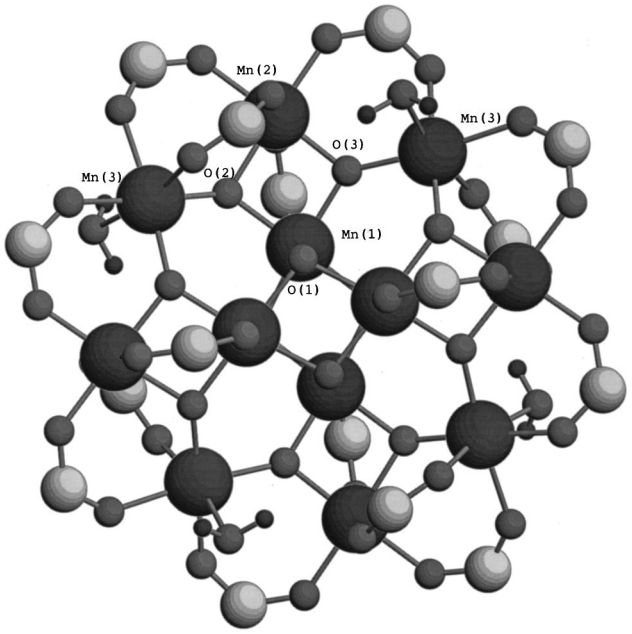

FIG. 2. Representation of $Mn_{12}(CH_3COO)_{16}(H_2O)_4O_{12}$, minus CH_3 ligands. Atoms are represented by spheres according to relative sizes: Mn>C>O>H. Types of Mn and O are indicated.

from which the CH_3 ligands have been removed to facilitate the calculation. This simplification is justified for our purposes, since the methyl ligands are peripheric, and sufficiently removed from the magnetic Mn atoms in the core, where our attention is focused. Since the CH_3—COO bonds that were truncated are covalent, upon the truncation each fragment was assumed to carry one electron of the electron pair of the bond, thus preserving charge neutrality.

According to a model inferred from experimental evidence,[11] the spins of the four Mn atoms [labeled Mn(1)] that form the inner cubane structure (see Fig. 1) were considered to align ferromagnetically among themselves, and antiferromagnetically to the eight outer Mn atoms, labeled Mn(2) and Mn(3), and this magnetic configuration was assumed throughout the self-consistent calculations. Mn(2) and Mn(3) occupy crystallographically different sites and are located in different planes, occupying alternate positions around the inner cubane. The Mn atoms are linked by triply bridging O atoms (μ_3-O); the Mn(1) are linked to Mn(2) by one carboxylate bridge, and the Mn(2) atoms are linked with the Mn(3) by three independent carboxylate bridges.[9] One water molecule completes the octahedral environment of the Mn(3) atom. Since the Mn_{12} molecule has S_4 point symmetry, there are only three crystallographically different Mn atoms. In Fig. 2 a top view of the molecule evidencing the symmetry is depicted, showing the labels of the atoms. All Mn atoms have a distorted octahedral coordination.

In Table I are given the Mulliken atomic orbital populations (electron occupation) of the valence orbitals of Mn(1), Mn(2), and Mn(3), as well as the net charges on the atoms and magnetic moments (in μ_B) of the individual orbitals and the total. The charges are defined as (Z minus total population), where Z is the atomic number, and the magnetic moments are defined as the spin-up population minus spin-down. Here we have adopted the convention by which the four inner Mn(1) atoms have positive spins, and Mn(2) and Mn(3) have negative. It is seen from this table that the Mn atoms are essentially ionic, with very small $4s$ and $4p$ populations and large positive charges. However, the charges are far from the values +4 [Mn(1)] and +3 [Mn(2) and Mn(3)] that are generally assumed based on simple chemical arguments.[9,11] The simple picture of configurations $3d^3_\uparrow 3d^0_\downarrow$ for Mn(1) and $3d^4_\uparrow 3d^0_\downarrow$ for Mn(2) and Mn(3) is found to be unrealistic, due to significantly higher occupation of both spin-up and spin-down orbitals, especially for Mn(1). In fact, the latter atoms may be expected to mix their wave functions more with those of their neighbors, since they occupy inner positions in the molecular aggregate. However, in spite of the smaller charges, the spin magnetic moments μ found are very similar to the expected values $3\mu_B$ for Mn(1) and $4\mu_B$ for Mn(2) and Mn(3), inferred from the simple model. The self-consistent total spin of the molecule is found to be 10, in agreement with magnetization and susceptibility measurements.[10,11] A further confirmation that the present spin configuration is correct was given by performing test calculations for other spin configurations, namely (1) Mn(2) spin up and Mn(1), Mn(3) spin down; (2) Mn(3) spin up, Mn(1), Mn(2) spin down. In both cases, the total spin of the molecule obtained was considerably smaller than ten disagreeing with the experimental finding.

In Table I are also given the values of the charges and magnetic moments of the oxygen atoms of type O(1), O(2), and O(3) that link the Mn atoms, and of the oxygen atoms of the ligand water molecules and carboxylates. Data on the C atoms are not given since these are not very well described, due to the truncated bonds with CH_3. As expected, the negative charges on the O atoms increase with increasing ionicity

TABLE I. Mulliken populations, charges, and magnetic moments of Mn_{12}. Charges are defined as (Z minus total population), where Z is atomic number. The magnetic moment is defined as total population of spin-up minus total population of spin down. Small differences from atomic values for $3s$ and $3p$, included in basis, are not given here.

		Populations			
		Spin ↑	Spin ↓	Spin ↑+Spin ↓	Spin ↑−Spin ↓
Mn(1)	$3d$	3.844	0.795	4.638	3.049
	$4s$	0.008	0.004	0.012	0.005
	$4p$	0.013	0.011	0.023	0.002
Mn(2)	$3d$	0.442	4.314	4.755	−3.872
	$4s$	0.009	0.024	0.033	−0.015
	$4p$	0.014	0.016	0.030	−0.002
Mn(3)	$3d$	0.361	4.391	4.752	−4.030
	$4s$	0.008	0.016	0.024	−0.008
	$4p$	0.016	0.017	0.032	−0.001
			Charge	Magnetic moment (μ_B)	
Mn(1)			2.34	3.056	
Mn(2)			2.20	−3.889	
Mn(3)			2.21	−4.039	
O(1)			−1.24	−0.077	
O(2)			−1.38	0.027	
O(3)			−1.31	0.023	
O(COO) (average)			−1.02	±0.039	
$O(H_2O)$			−1.55	−0.010	

of the bonds which they form, the oxygen in H_2O having the largest negative charge and the O atoms of the carboxylates, which form covalent bonds with C, the smallest. An interesting feature obtained is the very small spin magnetic moments of the oxygens, all having magnitude $<0.08\mu_B$. This is in complete disagreement with the results obtained from powder neutron-diffraction experiments performed on Mn_{12}, which give a moment of magnitude $1.0\mu_B$ on O(2) and O(3).[14] We believe that the modeling of the observed magnetic diffraction intensities may have induced some error in the derived moments. Besides the discrepancy with our first-principles calculations, the observation of such large induced moments would be an extraordinary event.

In Figs. 3(a), 3(b), and 3(c) are depicted the projected density of states (DOS) diagrams for Mn(1), Mn(2), and Mn(3), respectively. DOS diagrams may be constructed from the dense band of discrete energy levels of the molecule by broadening these levels with Lorentzians:[30]

$$\mathrm{DOS}^q_{nl\sigma}(\varepsilon)=\Sigma_i P^q_{nl\sigma i}\frac{\delta/\pi}{(\varepsilon-\varepsilon_{i\sigma})^2+\delta^2}, \tag{5}$$

where $P^q_{nl\sigma i}$ is the Mulliken population of atomic orbital χ_{nl} of atom q in the molecular spin orbital $\varphi_{i\sigma}$ and δ is the half-width of the Lorentzian, here taken as 0.14 eV. By summing over n, l and i the projected DOS of spin σ for atom q is obtained.

The DOS of Mn(1) shows a narrow peak just below the Fermi level of spin up, and a corresponding spin-down peak just above the Fermi level. Practically all the levels contributing are $3d$, since the $4s$ and $4p$ have very small populations. We can see the splitting induced by the crystal field of the ligands in the distorted octahedral arrangement, which is much larger in the spin-down peak. A band of lower DOS extending to ~8 eV below the Fermi energy results from the bond formation with the oxygens, since the O levels pertain to this region. To illustrate this point, we show in Figs. 4(a), 4(b), and 4(c) the DOS diagrams for the valence levels of O(1), O(2), and O(3), respectively, which also extend to about 8 eV below the Fermi level; practically only the O $2p$ levels contribute to the DOS in this region.

The DOS diagrams for Mn(2) and Mn(3) are similar to Mn(1), except that the lower energy bonding region shows significantly lower DOS values. This is understandable considering, as mentioned earlier, that the Mn(1) atoms are at the center of the molecular cluster.

In Figs. 5(a) and 5(b) are displayed the total electron density $\rho(\mathbf{r})$ and the spin density $\rho_\uparrow(\mathbf{r})-\rho_\downarrow(\mathbf{r})$, in a plane containing two Mn(1) atoms of the cubane center and two Mn(2) (see Figs. 1 and 2 for visualization). In this plane the bonding between Mn(1) and O(1) in the cubane unit results in mixture of the positive spin density of these atoms. In all other cases, the Mn atoms attract to their vicinity spin density of opposite sign from the neighboring oxygens. In Figs. 6(a) and 6(b) are shown the total density and spin density, respectively, in a plane perpendicular to the symmetry axis and containing two Mn(1) and two Mn(2) (see Fig. 2 for better visualization). In this plane, the oxygen spin density in the vicinity of the spin density of the Mn atoms is always of opposite sign. From these maps it becomes clear why the oxygen net magnetic moments are so small: they result from

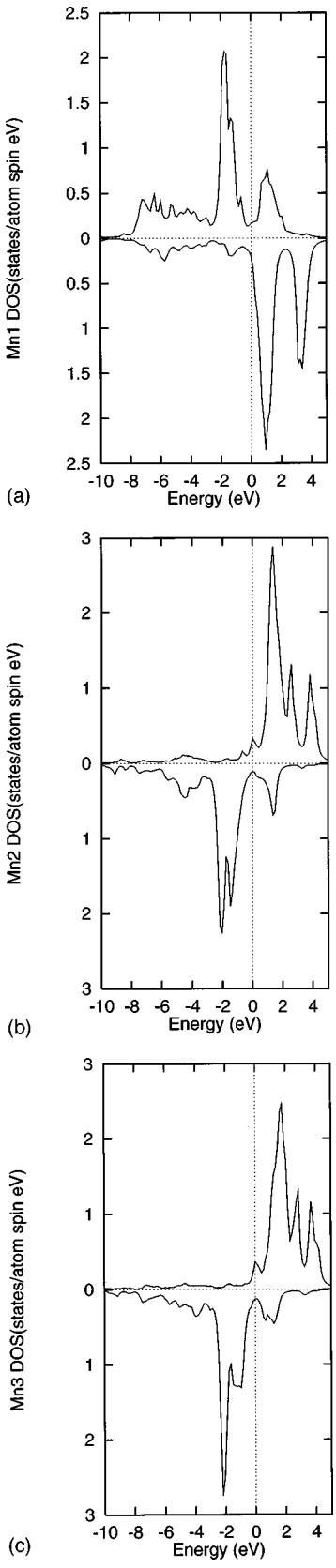

FIG. 3. (a) Total valence $(3d+4s+4p)$ DOS of Mn(1) in Mn_{12}. Fermi level has been shifted to zero energy. Upper part of figure is spin up DOS, lower part is spin down. (b) Total valence $(3d+4s+4p)$ DOS of Mn(2). (c) Total valence $(3d+4s+4p)$ DOS of Mn(3). Contributions of $4s$ and $4p$ are very small.

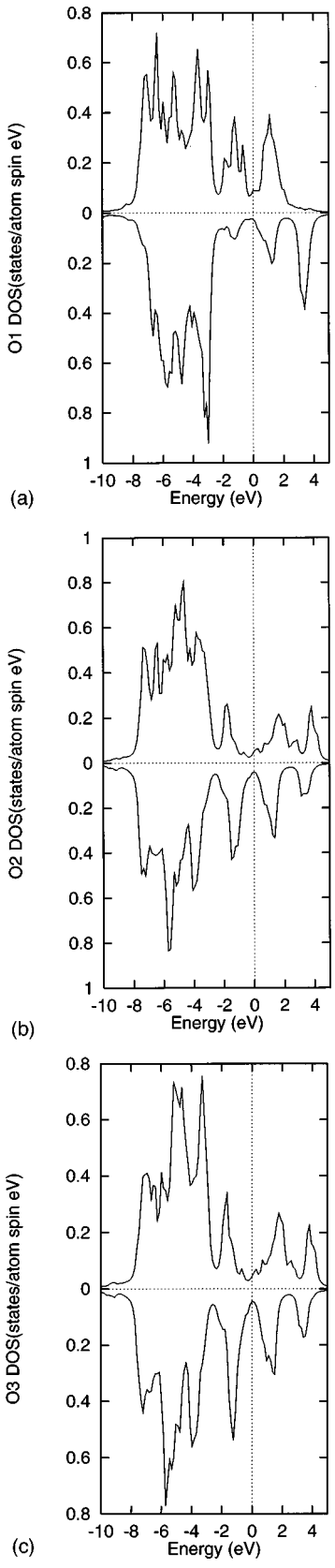

FIG. 4. (a) Total valence $(2s+2p)$ DOS of O(1) in Mn_{12}. Fermi level has been shifted to zero energy. Upper part of figure is spin up DOS, lower part is spin down. (b) Total valence $(2s+2p)$ DOS of O(2). (c) Total valence $(2s+2p)$ DOS of O(3). Contribution of $2s$ is small in this region.

the combination of positive and negative $2p$-orbital spin densities on each O atom. The reader must also keep in mind that the plotting parameters utilized for the contour maps are such that even very small densities in-between the Mn atoms are represented (see captions of Figs. 5 and 6).

B. Calculation of the Heisenberg exchange parameter *J*

The Heisenberg exchange Hamiltonian is a convenient representation of magnetic interactions between pairs of ions, much used to fit experimental susceptibility and spectroscopic data. In favorable cases it is capable of giving an accurate fit to energy differences between different spin states of rather complex systems. Therefore, it is interesting to calculate magnetic energy differences from first principles, and then to project these energies onto the Heisenberg scheme, in order to compare with experiment and also to obtain a simple interpretation of the interactions. In Mn-O systems, indirect superexchange interactions, mediated by the polarized oxygen ligands, dominate the Mn-Mn spin coupling; nevertheless, well-defined J values for Mn-Mn pairs were obtained from experimental susceptibilities for molecules containing small Mn-O groups.[6] The complexity of the present molecule Mn_{12} has not allowed the determination of J values from experiment;[11] therefore, it is useful to extract values for this parameter from first-principles calculations. By treating the Mn(1), Mn(2), and Mn(3) groups as rigidly coupled spins we are able to extract the coupling parameters J_{12} [for a Mn(1)-Mn(2) pair], J_{13} [for a Mn(1)-Mn(3) pair], and J_{23} [for a Mn(2)-Mn(3) pair].

We briefly describe the magnetic transition state (MTS) procedure used here to calculate magnetic energy differences from first principles. Details of Slater's transition state scheme[31] and the derived MTS procedure[24] are given in the original references. By expanding the density-functional total energy in powers of the orbital occupation numbers, one obtains the basic equation

$$\Delta E = \Sigma_i \Delta n_i \varepsilon_i^* + O(\Delta n^3), \tag{6}$$

where Δn_i are differences between occupation number in initial state and final state, and ε_i^* are the TS eigenvalues, obtained from a self-consistent-field calculation with occupation numbers midway between initial and final states.[31] In a variety of applications the TS scheme has been found to give a rather accurate account of electronic relaxation in the excited state, although, of course, it does not include geometric relaxation of nuclear positions as formulated. The TS procedure is highly useful in that it is a *differential* procedure capable of directly determining energy differences in a single self-consistent calculation, without the need of subtracting large (and numerically uncertain) total energies.

In the case of localized magnetic transitions, further elaboration of the TS scheme is possible, since the chemical state of the system hardly changes, and the character of the changes in occupation Δn_i are predetermined. We may now specialize to the case of a spin flip at a defined atomic site A, with the rest of the system undisturbed. This flip requires an amount of energy ΔE, which is given by

$$\Delta E = \Sigma_i (n_{i\uparrow}^A - n_{i\downarrow}^A)(\varepsilon_{i\downarrow}^* - \varepsilon_{i\uparrow}^*). \tag{7}$$

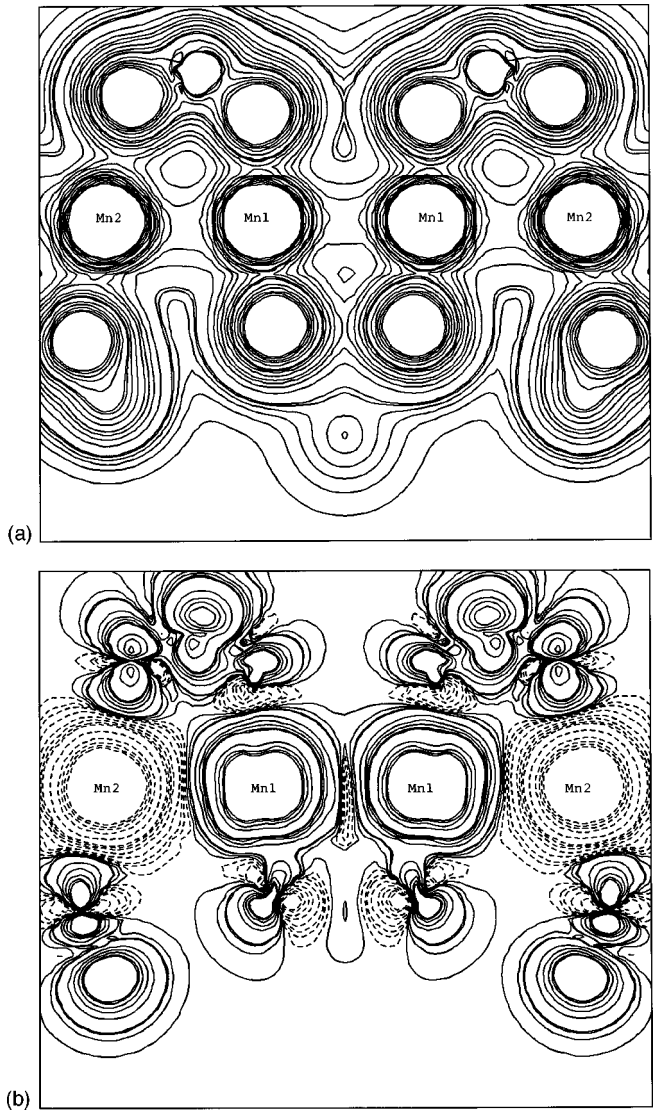

FIG. 5. (a) Electron density $\rho(r)$ contours of Mn_{12} in plane containing molecular axis and including two Mn(1) and two Mn(2) (see Fig. 1). Contours are from 0.001 to $0.01e/a_0^3$, with intervals $0.002e/a_0^3$; from 0.01 to $0.05e/a_0^3$ with intervals $0.01e/a_0^3$; from 0.05 to $0.12e/a_0^3$ with intervals $0.02e/a_0^3$; from 0.12 to $0.4e/a_0^3$ with intervals $0.05e/a_0^3$. (b) Spin density $\rho_\uparrow(\mathbf{r})-\rho_\downarrow(\mathbf{r})$ contours of Mn_{12} in plane containing molecular axis and including two Mn(1) and two Mn(2) (see Fig. 1). Contours are from 0.0001 to $0.001e/a_0^3$, with intervals $0.0004e/a_0^3$; from 0.001 to $0.01e/a_0^3$, with intervals $0.002e/a_0^3$; from 0.01 to $0.1e/a_0^3$, with intervals $0.02e/a_0^3$; from -0.1 to $-0.01e/a_0^3$, with intervals $0.02e/a_0^3$; from -0.01 to $-0.001e/a_0^3$, with intervals $0.002e/a_0^3$; from -0.001 to $-0.0001e/a_0^3$, with intervals $0.0004e/a_0^3$. Full lines are positive values.

Equation (7) follows from Eq. (6), with $n_{i\sigma}^A$ being the occupancy at site A of orbital $(i\sigma)$ in the *initial state*. This equation permits a simple interpretation of the MTS and the reason for its numerical precision: In the MTS Hamiltonian, the spin flip results in zero net spin on site A (the ''transition state'' between spin up and spin down); thus the magnetic energy difference at site A is due to ''external'' fields. If we suppose that the orbital magnetic splitting is nearly constant, then

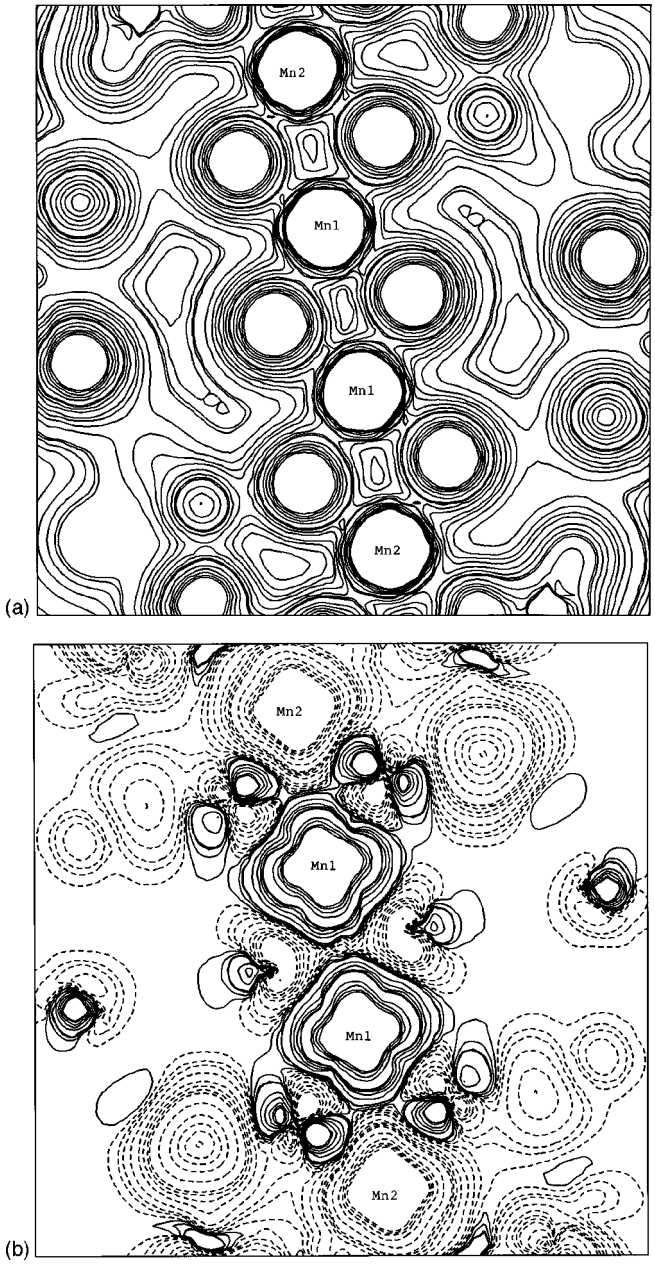

FIG. 6. (a) Electron density $\rho(\mathbf{r})$ contours of Mn_{12} in plane perpendicular to molecular axis and including two Mn(1) and two Mn(2) (see Fig. 2). Contours are from 0.001 to $0.01e/a_0^3$, with intervals $0.002e/a_0^3$; from 0.01 to $0.05e/a_0^3$ with intervals $0.01e/a_0^3$; from 0.05 to $0.12e/a_0^3$ with intervals $0.02e/a_0^3$; from 0.12 to $0.4e/a_0^3$ with intervals $0.05e/a_0^3$. (b) Spin density $\rho_\uparrow(\mathbf{r})-\rho_\downarrow(\mathbf{r})$ contours of Mn_{12} in plane perpendicular to molecular axis and including two Mn(1) and two Mn(2) (see Fig. 2). Contours are from 0.0001 to $0.001e/a_0^3$, with intervals $0.0004e/a_0^3$; from 0.001 to $0.01e/a_0^3$, with intervals $0.002e/a_0^3$; from 0.01 to $0.1e/a_0^3$, with intervals $0.02e/a_0^3$; from -0.1 to $-0.01e/a_0^3$, with intervals $0.02e/a_0^3$; from -0.01 to $-0.001e/a_0^3$, with intervals $0.002e/a_0^3$; from -0.001 to $-0.0001e/a_0^3$, with intervals $0.0004e/a_0^3$. Full lines are positive values.

$$(\varepsilon_{i\downarrow}^*-\varepsilon_{i\uparrow}^*)\cong\mu_B H_0, \tag{8}$$

and the total-energy difference reduces to the classical result $\Delta E=M^A H_0$ with

TABLE II. Ground-state magnetic moments, transition-state energy splittings, and Heisenberg J parameters of Mn_{12}.

	$(N^A_\uparrow - N^A_\downarrow)$ (Ground state, in μ_B)	$(\varepsilon^*_{1\downarrow} - \varepsilon^*_{1\uparrow})$ (MTS, in eV)
Mn(1)	+3.056	+0.2396
Mn(2)	−3.889	+0.0871
Mn(3)	−4.039	+0.0756
Heisenberg exchange parameters (cm^{-1})		
	J_{12}	−94.3
	J_{13}	−50.1
	J_{23}	−70.8

$$M^A = (N^A_\uparrow - N^A_\downarrow)\mu_B , \tag{9}$$

where N^A_σ is the total initial state population of spin σ in site A.

Operationally, the MTS self-consistent calculation is one for which in each cycle the exchange potential is set to zero for site A. When the potential of the molecule stabilizes, a small magnetic moment is left on A, which is exclusively the result of the polarization induced by the moments on the other sites. For the present complex system, direct application of Eq. (7) is cumbersome due to the difficulty in identifying each level in the ground state with its counterpart in the MTS, amidst the dense mass of valence levels. Further simplification reduces Eq. (7) to

$$\Delta E = (N^A_\uparrow - N^A_\downarrow)(\varepsilon^*_{A\downarrow} - \varepsilon^*_{A\uparrow}), \tag{10}$$

in which $\varepsilon^*_{A\sigma}$ is the center or average energy of the spin σ ''band'' in the MTS calculation. Projected density of states (PDOS) diagrams are extremely useful in identifying the relevant magnetic orbitals amidst the sea of valence states. The four Mn ions of each magnetic type in fact generate a $3d$ PDOS of significant width, consisting of a ''crystal field'' band of width ~1.5 eV, bonding structure spread over the oxygen valence band of width ~6 eV, and unoccupied antibonding structure extending well above E_F. The occupation numbers in the MTS equation serve to exclude all states in which both spins are initially occupied, or both spins are initially unoccupied. The result is that the exchange-split crystal-field states which bracket E_F are the only ones which contribute to ΔE. We have thus calculated the band center or average energy of the spin ↑,↓ crystal-field bands to define a single (average) magnetic energy difference. These energies are reported in Table II, along with the ground-state moments $N^A_\uparrow - N^A_\downarrow$.

Next we briefly describe the method used to determine J_{ij}, which is similar to that used by other authors in theoretical calculations for smaller Mn-O molecules,[32,33] in which linear equations are developed to fit to calculated magnetic energy differences. Taking the definition

$$H = -2\Sigma_{i<j} J_{ij} S_i \cdot S_j , \tag{11}$$

we consider the sets (1), (2), and (3) each containing four Mn with spins rigidly coupled ferromagnetically among themselves. By considering spin orientations $M_S = \pm S$ sufficient state energies can be obtained to determine the J values. In the self-consistent calculations M_S is a well-defined quantum number, while the total spin S is undetermined. As is well known, in both Hartree-Fock and DFT spin-polarized methods there is a mixture of states with $S \geq M_S$. In general, the lower value of S dominates and we simply take $S = |M_S|$ in the following analysis.

Let us denote by $\langle H_A \rangle$ the expectation value of H, expressed in terms of the interaction of ion type ''A'' with the other two types, then the magnetic excitation energy for type ''A'' is $\Delta E_A = \langle H_A \rangle^{\mathrm{FM}} - \langle H_A \rangle^{\mathrm{AFM}}$. Here ferromagnetic (FM) and antiferromagnetic (AFM) refer to the two extreme alignments of spins of type A, with spin moments determined from the self-consistent-field calculations, for ground state (AFM) and excited (FM, spin-flip) state. It is important to note that, different from other workers, we have *not* assumed for Mn the formal ionic spins of 3/2 and 2 in this procedure but have used the first-principles moments. Using the trivial result $\langle S_A \cdot S_B \rangle^{\mathrm{FM}} - \langle S_A \cdot S_B \rangle^{\mathrm{AFM}} = 1/2[(S_A + S_B)(S_A + S_B + 1) - |S_A - S_B|(|S_A - S_B| + 1)]$ we obtain three linear equations for the J_{ij}:

$$\begin{aligned}
\Delta E_1 &= -8J_{12}[S^{\mathrm{FM}}(S^{\mathrm{FM}}+1) - S^{\mathrm{AFM}}(S^{\mathrm{AFM}}+1)]_{1,2} \\
&\quad -16J_{13}[S^{\mathrm{FM}}(S^{\mathrm{FM}}+1) - S^{\mathrm{AFM}}(S^{\mathrm{AFM}}+1)]_{1,3}, \\
\Delta E_2 &= -8J_{12}[S^{\mathrm{FM}}(S^{\mathrm{FM}}+1) - S^{\mathrm{AFM}}(S^{\mathrm{AFM}}+1)]_{1,2} \\
&\quad -16J_{23}[S^{\mathrm{FM}}(S^{\mathrm{FM}}+1) - S^{\mathrm{AFM}}(S^{\mathrm{AFM}}+1)]_{2,3}, \\
\Delta E_3 &= -8J_{13}[S^{\mathrm{FM}}(S^{\mathrm{FM}}+1) - S^{\mathrm{AFM}}(S^{\mathrm{AFM}}+1)]_{1,3} \\
&\quad -16J_{23}[S^{\mathrm{FM}}(S^{\mathrm{FM}}+1) - S^{\mathrm{AFM}}(S^{\mathrm{AFM}}+1)]_{2,3}
\end{aligned} \tag{12}$$

(in the notation of Ref. 11, J_{12} is J_1, J_{13} is J_2, and J_{23} is J_4). Subscripts on the square brackets denote pairs of spin types 1, 2, and 3, and FM (AFM) indicates parallel (antiparallel) combinations of the given spin pairs. Multiplication factors 8 and 16 derive from the fact that each of the four Mn(1) has one Mn(2) and two Mn(3) nearest neighbors, and Mn(2) has two Mn(3) (see Ref. 11 for schematics). The values of J are then obtained by combining Eqs. (10) and (12) for each type of Mn. The calculated values of J_{ij}, given in Table II, are within the range of experimentally fitted values for other (smaller) Mn-O molecules.[6] Effects of varying the computational procedure, such as the manner of determining the magnetic band-average energy, and uncertainty in position of Fermi energy due to basis set choice, integration mesh of self-consistent field calculations, choice of exchange-correlation potential, etc. have been considered. We estimate an overall uncertainty of ±20% in J values, which would not alter the sign (all interactions are <0; i.e., AFM in nature).

The relative magnitudes of the pairwise exchange interactions determine which ground state is present.[6] Since all three values of J are negative, the spins of Mn in different groups would tend to be paired; however, since the molecular geometry does not allow such configurations, considerable spin frustration is generated. Due to symmetry constraints, as mentioned above, we could not obtain the coupling parameter J_{11} for Mn(1)-Mn(1), which may also be expected to be negative and, as such, induce more frustation

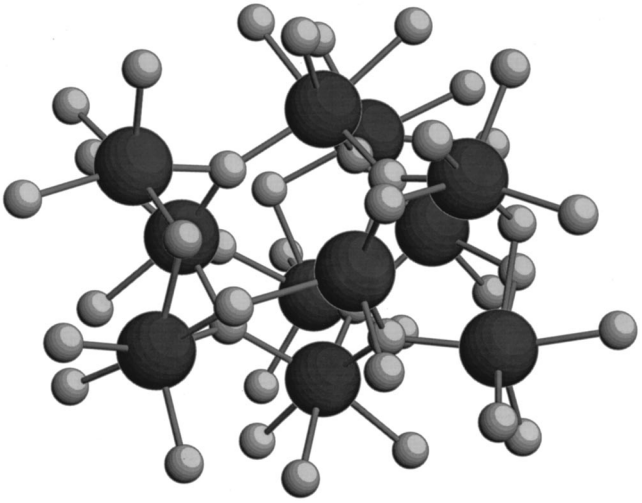

FIG. 7. Representation of Fe-O core of $Fe_{11}O_6(OH)_6(O_2CPh)_{15}$. Larger spheres represent Fe, smaller spheres represent O.

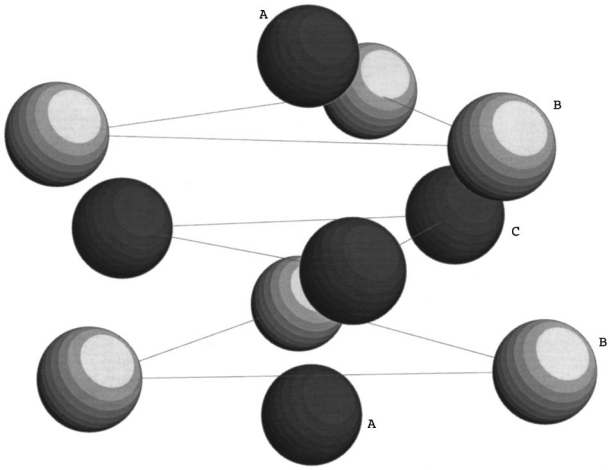

FIG. 8. Fe atoms in $Fe_{11}O_6(OH)_6(O_2CPh)_{15}$. Dark shade spheres are atoms with positive spin, light shade are negative spin.

in the coupling of Mn(1) with Mn(2) and Mn(3). Neglect of J_{11} will have induced further error in the solution of the coupled equations.

The J values calculated here reflect the superexchange interactions mediated by the oxygens. Another type of magnetic interaction may be considered between Mn($S=3/2$) and Mn($S=2$), that is, between Mn(1) and Mn(2,3), usually known as ''double exchange'' which would induce ferromagnetic coupling.[34] However, the chemical environment of the Mn groups are different and this results in some ''quenching'' of this effect.

IV. THE Fe OXO-HYDROXO AGGREGATE $Fe_{11}O_6(OH)_6(O_2CPh)_{15}$

As cited previously, the structure of Fe_{11} has been determined by x-ray diffraction;[20] the experimentally obtained atomic coordinates reported in the literature (rhombohedral crystalline form) were used in the present calculations.

In Fig. 7 is depicted the Fe-O core of the molecule Fe_{11}, which was stripped of all organic ligands to render the calculations feasible. The organic ligands were substituted by hydrogen, a procedure known as ''hydrogen saturation;'' this assures that the valence capacity of the O atoms will be fullfilled. Magnetic and Mössbauer studies[20] indicate strong coupling of the spins within each molecule, which may thus be viewed as a nanoscale magnet, and antiferromagnetic alignment of the magnetic moments, for which layers of spin-up and spin-down Fe atoms is a reasonable model, as represented in Fig. 8. There are three crystallographically different Fe sites in the molecule, here denominated (as in Ref. 20) A (the two atoms at the top and bottom of the cluster in Fig. 8, dark shade), B (six outermost atoms, light shade), and C (three innermost atoms, dark shade). The convention we adopted assigns positive spins for the A and C layers, and negative for B.

In Table III are given the populations, charges and mag-

TABLE III. Mulliken populations, charges and magnetic moments of Fe_{11}. Charges are defined as (Z minus total population), where Z is atomic number. Magnetic moment is defined as total population of spin up minus total population of spin down. Small differences from atomic values for $3s$ and $3p$, included in basis, are not given here.

		Populations			
		Spin ↑	Spin ↓	Spin ↑+Spin ↓	Spin ↑−Spin ↓
Fe(A)	$3d$	4.873	0.865	5.738	4.008
	$4s$	0.006	0.004	0.010	0.002
	$4p$	0.008	0.005	0.013	0.003
Fe(B)	$3d$	1.204	4.715	5.919	−3.511
	$4s$	0.033	0.071	0.103	−0.038
	$4p$	0.037	0.058	0.095	−0.021
Fe(C)	$3d$	4.778	1.359	6.136	3.419
	$4s$	0.072	0.044	0.116	0.028
	$4p$	0.050	0.040	0.090	0.010
			Charge	Magnetic moment (μ_B)	
Fe(A)			2.25	4.013	
Fe(B)			1.67	−3.570	
Fe(C)			1.90	3.457	

netic moments of the Fe atoms. The $4s$ and $4p$ populations are quite small, specially for Fe type *A*. The charges found are smaller than the formal value $+3$, and the magnetic moments have values lower than the Fe(III) ion with formal configuration $3d^5 4s^0$. In Figs. 9(a), 9(b), and 9(c) are displayed the total valence DOS diagrams (constituted almost totally of $3d$) projected onto Fe sites *A*, *B*, and *C*. Considerable structure is seen in the DOS, which is more pronounced for sites *A* and *B*, indicating strong admixture with the oxygen $2p$ wave functions.

Mössbauer hyperfine parameters[35] may be calculated with the self-consistent densities obtained with the DV method.[21] The isomer shift (IS) measured by Mössbauer spectroscopy is defined as

$$\mathrm{IS} = 2/3 e^2 \pi Z S'(Z) \Delta\langle r^2\rangle [\rho_A(0) - \rho_S(0)], \qquad (13)$$

where $\Delta\langle r^2\rangle$ is the variation of the mean-square radius of the nucleus between the excited and ground states of the Mössbauer transition, $S'(Z)$ is a correction for relativistic effects and the term in brackets is the difference between the electron density at the nucleus in the absorber *A* and source *S*. In a nonrelativistic approximation, only orbitals containing Fe-s states contribute to $\rho(0)$. For ^{57}Fe, a correlation between $\rho(0)(3s+4s)$ and IS values for free atom and ions gave $\mathrm{IS} = -0.228\rho(0) + 33.638$, with IS in mm/s and $\rho(0)$ in atomic units.[36]

The quadrupole splitting (QS) of the excited state of the 14.4 keV transition of ^{57}Fe is given by

$$\mathrm{QS} = 1/2 e V_{zz} Q (1 + \eta^2/3)^{1/2}, \qquad (14)$$

where Q is the quadrupole moment of the nucleus in the excited state ($I = 3/2$) of the Mössbauer transition, V_{zz} is the electric-field gradient and η is the asymmetry parameter, which is zero for axial symmetry. The components of the electric-field gradient tensor are calculated from the self-consistent molecular density by

$$V_{ij} = -e \int \rho(\mathbf{r})(3x_i x_j - \delta_{ij} r^2)/r^5 dv + \Sigma_q Z_q^e (3x_{qi} x_{qj} - \delta_{ij} r_q^2)/r_q^5. \qquad (15)$$

The first term is the valence electronic contribution and the second term is the contribution of the surrounding nuclei of the cluster or molecular atoms, with effective charge Z_q^e equal to the number of protons minus the number of core electrons. After diagonalization, necessary in the absence of axial symmetry, the electric-field gradient is defined by the convention

$$|V_{zz}| > |V_{yy}| \geq |V_{xx}| \qquad (16)$$

with asymmetry-parameter $\eta = (V_{xx} - V_{yy})/V_{zz}$. The value of Q employed was $0.16b$, obtained from combination of first-principles band-structure calculations and experiment in solids.[37]

The contact or Fermi component H_c of the magnetic hyperfine field H_F, which is usually the dominant component, is given by

$$H_c = (8/3)\pi \mu_B [\rho_\uparrow(0) - \rho_\downarrow(0)], \qquad (17)$$

where μ_B is the Bohr magneton and the term in brackets is the spin density at the nucleus.

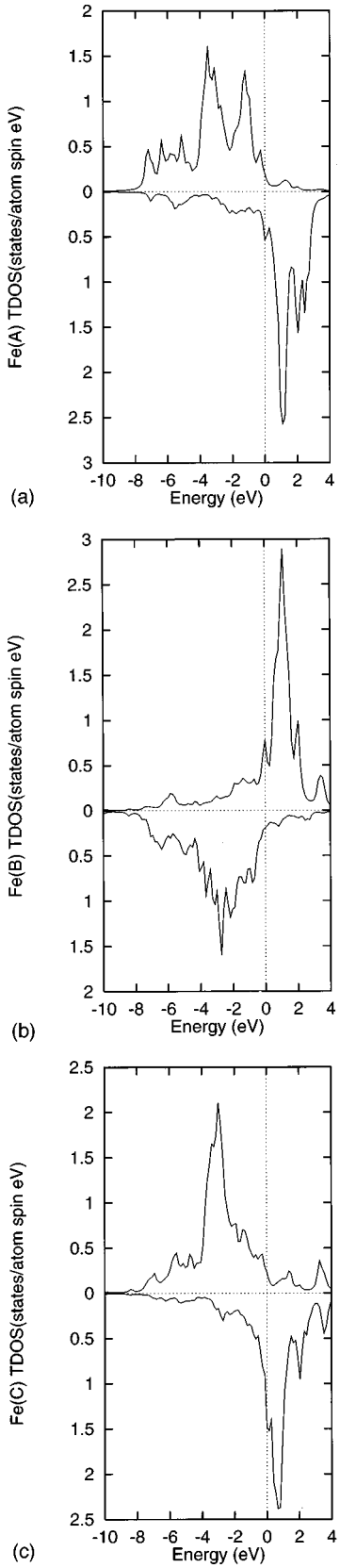

FIG. 9. (a) Total valence $(3d+4s+4p)$ density of states (TDOS) of Fe(A) in Fe_{11}. Fermi level has been shifted to zero energy. Upper part of figure is spin up TDOS, lower part is spin down. (b) Total valence $(3d+4s+4p)$ density of states (TDOS) of Fe(B). (c) Total valence $(3d+4s+4p)$ density of states (TDOS) of Fe(C). Contributions of $4s$ and $4p$ are small.

TABLE IV. Calculated and experimental hyperfine parameters of Fe_{11}.

	IS (mm/s)		QS (mm/s)[b]		H_c (kOe)	
	Calc.	Expt.[a]	Calc.	Expt.[a]	Calc.	Expt.[a]
Fe(A)	0.66	0.53	−0.77	0.49	−668	
Fe(B)	0.45	0.46	−0.82	0.87	+505	430
Fe(C)	0.71	0.51	−1.32	1.10	−400	

[a]From Ref. 20; the signs of QS and H_c were not determined.
[b]Value of $Q=0.16b$ from Ref. 37.

In Table IV the calculated hyperfine parameters are displayed, along with the experimental values.[20] The IS values compare reasonably well with experiment. The quadrupole splittings are found to be all negative (the sign was not determined experimentally) and the magnitudes are in good accord with the measured values. The magnitudes of the calculated hyperfine fields on Fe sites A and B are higher than the average value 430 kOe found experimentally, for which no sign was determined but may be expected to be negative for a positive Fe moment.

V. CONCLUSIONS

The electronic structure calculations performed for the nanoscale magnetic molecule Mn_{12} within an antiferromagnetic configuration confirmed the value of the total spin $S=10$ derived from experiments. Magnetic moments of the individual Mn atoms were found to be $3.05\mu_B$ for Mn(1), $-3.89\mu_B$ for Mn(2) and $-4.04\mu_B$ for Mn(3). Charges on the Mn are somewhat higher than +2, smaller than the charges +3 and +4 predicted by simple chemical arguments. The oxygen magnetic moments are very small, in contradiction with values derived from a fit to powder neutron-diffraction data.[14] Calculations of the Heisenberg exchange parameters J from first principles gave values that are within the range of experimentally derived values for smaller Mn-O molecules.

Calculations for the nanoscale molecular aggregate Fe_{11} within an AFM configuration revealed charges of $\sim+2$ on the Fe ions, smaller than the formal charge +3. Magnetic moments found are $4.01\mu_B$ for Fe(A), $-3.57\mu_B$ for Fe(B), and $3.46\mu_B$ for Fe(C), far from the conventional $5\mu_B$ of Fe(III) ions. Density of states diagrams reveal considerable mixture of the Fe valence functions (mainly $3d$) with the O $2p$. Calculated hyperfine parameters agree reasonably well with experimental values.

ACKNOWLEDGMENTS

Calculations were performed at the Cray Y-MP of the Supercomputing Center of the Universidade Federal do Rio Grande do Sul, Brazil. D.E.E. acknowledges support from the National Science Foundation Grant No. INT-9600016 and through the MRSEC program at the Northwestern University Materials Science Center, Grant No. DMR-9632472. Z. Zeng acknowledges support from the National Science Foundation of China (NSFC), Grant No. 19774058, from Pan Deng projects of 95-Yu-41 and Nanoscale Materials. D. Guenzburger acknowledges support from international Grant No. 910.154/95-3 from CNPq (CNPq/NSF collaboration).

[1] G. Blondin and J. J. Girerd, Chem. Rev. **90**, 1359 (1990), and references therein.
[2] A. Caneschi, D. Gatteschi, and R. Sessoli, J. Chem. Soc. Dalton Trans. **1997**, 3963 (1997), and references therein.
[3] T. G. St. Pierre, P. Chan, K. R. Bauchspiess, J. Webb, S. Betteridge, S. Walton, and D. P. E. Dickson, Coord. Chem. Rev. **151**, 125 (1996); J. M. A. Smith and J. R. Helliwell, Inorg. Chim. Acta **106**, 193 (1985); S. Mann, J. V. Bannister, and R. J. P. Williams, J. Mol. Biol. **188**, 225 (1986).
[4] G. C. Papaefthymiou, Phys. Rev. B **46**, 10 366 (1992); A. K. Powell, S. L. Heath, D. Gatteschi, L. Pardi, R. Sessoli, G. Spina, F. Del Giallo, and F. Pieralli, J. Am. Chem. Soc. **117**, 2491 (1995).
[5] D. D. Awschalom and D. P. DiVincenzo, Phys. Today **48**(4), 43 (1995); D. D. Awschalom, D. P. DiVincenzo, and J. F. Smyth, Science **258**, 414 (1992); D. Gatteschi, A. Caneschi, L. Pardi, and R. Sessoli, *ibid.* **265**, 1054 (1994).
[6] D. N. Hendrickson, G. Christou, E. A. Schmitt, E. Libby, J. S. Bashkin, S. Wang, H.-L. Tsai, J. B. Vincent, P. D. W. Boyd, J. C. Huffman, K. Folting, Q. Li, and W. E. Streib, J. Am. Chem. Soc. **114**, 2455 (1992).
[7] E. A. Schmitt, L. Noodleman, E. J. Baerends, and D. N. Hendrickson, J. Am. Chem. Soc. **114**, 6109 (1992).
[8] X. G. Zhao, W. H. Richardson, J.-L. Chen, J. Li, L. Noodleman, H.-L. Tsai, and D. N. Hendrickson, Inorg. Chem. **36**, 1198 (1997).
[9] T. Lis, Acta Crystallogr., Sect. B: Struct. Crystallogr. Cryst. Chem. **36**, 2042 (1980).
[10] A. Caneschi, D. Gatteschi, R. Sessoli, A. L. Barra, L. C. Brunel, and M. Guillot, J. Am. Chem. Soc. **113**, 5873 (1991).
[11] R. Sessoli, H.-L. Tsai, A. R. Schake, S. Wang, J. B. Vincent, K. Folting, D. Gatteschi, G. Christou, and D. N. Hendrickson, J. Am. Chem. Soc. **115**, 1804 (1993).
[12] R. Sessoli, D. Gatteschi, A. Caneschi, and M. A. Novak, Nature (London) **365**, 141 (1993).
[13] A. Lascialfari, D. Gatteschi, F. Borsa, A. Shastri, Z. Jang, and P. Carretta, Phys. Rev. B **57**, 514 (1998).
[14] P. A. Reynolds, E. P. Gilbert, and B. N. Figgis, Inorg. Chem. **35**, 545 (1996).
[15] M. Hennion, L. Pardi, I. Mirebeau, E. Suard, R. Sessoli, and A. Caneschi, Phys. Rev. B **56**, 8819 (1997).
[16] M. R. Cheesman, V. S. Oganesyan, R. Sessoli, D. Gatteschi, and

A. J. Thomson, Chem. Commun. (Cambridge) **1997**, 1677 (1997).
[17] A. L. Barra, D. Gatteschi, and R. Sessoli, Phys. Rev. B **56**, 8192 (1997).
[18] J. R. Friedman, M. P. Sarachik, J. Tejada, and R. Ziolo, Phys. Rev. Lett. **76**, 3830 (1996).
[19] F. Lionti, L. Thomas, R. Ballou, B. Barbara, A. Sulpice, R. Sessoli, and D. Gatteschi, J. Appl. Phys. **81**, 4608 (1997).
[20] S. M. Gorun, G. C. Papaefthymiou, R. B. Frankel, and S. J. Lippard, J. Am. Chem. Soc. **109**, 3337 (1987).
[21] Z. Zeng, Y. Duan, and D. Guenzburger, Phys. Rev. B **55**, 12 522 (1997).
[22] G. S. Painter and D. E. Ellis, Phys. Rev. B **1**, 4747 (1970); D. E. Ellis, Int. J. Quantum Chem. **2S**, 35 (1968); A. Rosén, D. E. Ellis, H. Adachi, and F. W. Averill, J. Chem. Phys. **65**, 3629 (1976); D. E. Ellis and D. Guenzburger, Adv. Quant. Chem. (to be published).
[23] R. G. Parr and W. Yang, *Density Functional Theory of Atoms and Molecules* (Oxford University Press, New York, 1989); *Density Functional Theory of Molecules, Clusters and Solids*, edited by D. E. Ellis (Kluwer Academic, Dordrecht, 1995).
[24] V. A. Gubanov and D. E. Ellis, Phys. Rev. Lett. **44**, 1633 (1980).
[25] S. H. Vosko, L. Wilk, and M. Nusair, Can. J. Phys. **58**, 1200 (1980).
[26] A. H. Stroud, *Approximate Calculation of Multiple Integrals* (Prentice Hall, Englewood Cliffs, NJ, 1971).
[27] R. S. Mulliken, J. Chem. Phys. **23**, 1833 (1955); **23**, 1841 (1955).
[28] B. Delley and D. E. Ellis, J. Chem. Phys. **76**, 1949 (1982).
[29] M. Battocletti, H. Ebert, and H. Akai, Phys. Rev. B **53**, 9776 (1996).
[30] P.-L. Cao, D. E. Ellis, and A. J. Freeman, Phys. Rev. B **25**, 2124 (1982).
[31] J. C. Slater, *The Self-Consistent Field for Molecules and Solids* (McGraw-Hill, New York, 1974), Vol. IV.
[32] E. A. Schmitt, L. Noodleman, E. J. Baerends, and D. N. Hendrickson, J. Am. Chem. Soc. **114**, 6109 (1992).
[33] X. G. Zhao, W. H. Richardson, J.-L. Chen, J. Li, L. Noodleman, H.-L. Tsai, and D. N. Hendrickson, Inorg. Chem. **36**, 1198 (1997).
[34] J. B. Goodenough, Phys. Rev. **100**, 564 (1955).
[35] N. N. Greenwood and R. C. Gibb, *Mössbauer Spectroscopy* (Chapman and Hall, London, 1971).
[36] J. Terra and D. Guenzburger, J. Chem. Phys. **99**, 4935 (1995).
[37] P. Dufek, P. Blaha, and K. Schwarz, Phys. Rev. Lett. **75**, 3545 (1995).